2001-12

Validation of operational global wave prediction models with spectral buoy data

Wingeart, Karen M.

Monterey, California. Naval Postgraduate School

NAVAL POSTGRADUATE SCHOOL
Monterey, California

THESIS

VALIDATION OF OPERATIONAL GLOBAL WAVE PREDICTION MODELS WITH SPECTRAL BUOY DATA

by

Karen M. Wingeart

December 2001

Thesis Advisor: Thomas H.C. Herbers
Co-Advisor: Paul A. Wittmann

THIS PAGE INTENTIONALLY LEFT BLANK

REPORT DOCUMENTATION PAGE

Form Approved OMB No. 0704-0188

1. AGENCY USE ONLY *(Leave blank)*	2. REPORT DATE	3. REPORT TYPE AND DATES COVERED
	December 2001	Master's Thesis

4. TITLE AND SUBTITLE: Title (Mix case letters)
Validation of Operational Global Wave Prediction Models with Spectral Buoy Data

5. FUNDING NUMBERS

6. AUTHOR(S) Karen M. Wingeart

7. PERFORMING ORGANIZATION NAME(S) AND ADDRESS(ES)
Naval Postgraduate School
Monterey, CA 93943-5000

8. PERFORMING ORGANIZATION REPORT NUMBER

9. SPONSORING /MONITORING AGENCY NAME(S) AND ADDRESS(ES)
N/A

10. SPONSORING/MONITORING AGENCY REPORT NUMBER

11. SUPPLEMENTARY NOTES The views expressed in this thesis are those of the author and do not reflect the official policy or position of the Department of Defense or the U.S. Government.

12a. DISTRIBUTION / AVAILABILITY STATEMENT
Approved for public release; distribution is unlimited.

12b. DISTRIBUTION CODE

13. ABSTRACT ***(maximum 200 words)***

Global wave predictions produced at two U. S. forecasting centers, Fleet Numerical Meteorology and Oceanography Center and the National Centers for Environmental Prediction are evaluated with spectral buoy measurements. In this study, the fidelity of frequency-directional spectra predicted by WAM and WAVEWATCH III at the operational centers is examined with data from 3-meter discus and 6-meter nomad buoys operated by the National Data Buoy Center in the Atlantic and Pacific Oceans and Datawell Directional Waverider buoys deployed along the California coast by the Scripps Institution of Oceanography Coastal Data Information Program. Only buoys located in deep water are used in the comparisons. Model nowcasts of frequency spectra and mean wave directions are compared to buoy measurements over a six-month period from 1 October 2000 to 31 March 2001. At the Pacific buoy locations, individual swell events were identified in the spectra from the three models and the buoy data. Predicted and observed swell frequencies and arrival directions are compared as well as the total energy transported past the buoy over the duration of each individual event. At all buoy locations, predicted and observed wave energy fluxes integrated over fixed frequency ranges are compared. All three models yield reliable nowcasts of swell arrivals at the buoy locations. In most cases, the models under-predict the energy measured by the buoys. WAVEWATCH III better resolves low-frequency swells than WAM, possibly owing to a superior numerical scheme. Swell predictions at NCEP forced with AVN winds are more accurate than those at FNMOC forced with NOGAPS winds.

14. SUBJECT TERMS	15. NUMBER OF PAGES
Global Wave Prediction Models, WAM, WAVEWATCH III, swell, wave	57
	16. PRICE CODE

17. SECURITY CLASSIFICATION OF REPORT	18. SECURITY CLASSIFICATION OF THIS PAGE	19. SECURITY CLASSIFICATION OF ABSTRACT	20. LIMITATION OF ABSTRACT
Unclassified	Unclassified	Unclassified	UL

NSN 7540-01-280-5500

Standard Form 298 (Rev. 2-89)
Prescribed by ANSI Std. 239-18

THIS PAGE INTENTIONALLY LEFT BLANK

Approved for public release; distribution is unlimited.

VALIDATION OF OPERATIONAL GLOBAL WAVE PREDICTION MODELS WITH SPECTRAL BUOY DATA

Karen M. Wingeart
Lieutenant, United States Navy
B.S., United States Naval Academy, 1996

Submitted in partial fulfillment of the
requirements for the degree of

MASTER OF SCIENCE IN METEOROLOGY AND PHYSICAL OCEANOGRAPHY

from the

NAVAL POSTGRADUATE SCHOOL
December 2001

Author: _____
Karen M. Wingeart

Approved by: _____
Thomas H.C. Herbers, Advisor

_____
Paul A. Wittmann, Co-Advisor

_____
Mary L. Batteen, Chairman
Department of Oceanography

THIS PAGE INTENTIONALLY LEFT BLANK

ABSTRACT

Global wave predictions produced at two U. S. forecasting centers, Fleet Numerical Meteorology and Oceanography Center (FNMOC) and the National Centers for Environmental Prediction (NCEP) are evaluated with spectral buoy measurements. In this study, the fidelity of frequency-directional spectra predicted by WAM and WAVEWATCH III at the operational centers is examined with data from 3-meter discus and 6-meter nomad buoys operated by the National Data Buoy Center in the Atlantic and Pacific Oceans and Datawell Directional Waverider buoys deployed along the California coast by the Scripps Institution of Oceanography Coastal Data Information Program. Only buoys located in deep water are used in the comparisons. Model nowcasts of frequency spectra and mean wave directions are compared to buoy measurements over a six-month period from 1 October 2000 to 31 March 2001. At the Pacific buoy locations, individual swell events were identified in the spectra from the three models and the buoy data. Predicted and observed swell frequencies and arrival directions are compared at the Pacific buoy locations, as well as the total energy transported past the buoy over the duration of each individual event. At all buoy locations, predicted and observed wave energy fluxes integrated over fixed frequency ranges are compared. All three models yield reliable nowcasts of swell arrivals at the buoy locations. In most cases, the models under-predict the energy measured by the buoys. WAVEWATCH III better resolves low-frequency swells than WAM, possibly owing to a superior numerical scheme. Swell predictions at NCEP forced with AVN winds are more accurate that those at FNMOC forced with NOGAPS winds.

THIS PAGE INTENTIONALLY LEFT BLANK

TABLE OF CONTENTS

THIS PAGE INTENTIONALLY LEFT BLANK

LIST OF FIGURES

LIST OF TABLES

THIS PAGE INTENTIONALLY LEFT BLANK

ACKNOWLEDGMENTS

The author would like to acknowledge those without whose support this work would not have been possible:

To my advisor, Thomas Herbers, my deepest gratitude for all your patience and guidance throughout the past year and a half.

To my co-advisor, Paul Wittmann, my warmest thanks for all your help and understanding.

To Hendrik Tolman and Bill O'Reilly, my sincere thanks for all your help with the models and data.

To Paul Jessen and Mark Orzech, my sincere thanks for all your help with the computer work.

To my husband, Paul and my daughter, Aubrey, my love and appreciation for your patience and understanding.

THIS PAGE INTENTIONALLY LEFT BLANK

I. INTRODUCTION

Third generation wave prediction models that describe the evolution of the two-dimensional ocean wave spectrum are widely used in global and regional applications. The first of these models, WAM, was developed in 1988 by the WAMDI Group (WAMDI Group, 1988) and was adopted for operational use by the Fleet Numerical Meteorology and Oceanography Center (FNMOC) in 1994. It solves the wave action balance equation in spherical coordinates for a two-dimensional wave spectrum.

$$\frac{DE(f,\theta,\lambda,\phi,t)}{Dt} = S_{in} + S_{nl} + S_{ds} \tag{1}$$

where E is the action density as a function of wave frequency (f), propagation direction (θ), latitude (λ), longitude (ϕ), and time (t), and D/Dt is the total derivative following a wave group. The source function, S, represents the net rate of increase of the wave action of a spectral component resulting from wind input, non-linear interactions with other spectral components, and dissipation induced by wave breaking. The wind input source function (S_{in}) is scaled in terms of friction velocity u_* (Janssen, 1991), based on Charnock's original boundary layer model (WAMDI Group, 1988). The dissipation source function (S_{ds}) is a slight modification to the semi-empirical form that Komen et al. (1984) proposed, replacing the mean frequency by the inverse of the mean period to enhance the stability of the implicit integration scheme and enable a larger time step (WAMDI Group, 1988). The non-linear source function (S_{nl}) describes resonant quartet interactions with the simplified parameterization of the Boltzman interaction integral (Hasselmann et al., 1985). The model uses an implicit integration scheme for the source functions and a first-order upwind propagation scheme with a fixed time step of 20 minutes (WAMDI Group, 1988). The FNMOC WAM model is forced by the Navy's atmospheric prediction system NOGAPS 3.4 surface wind stress.

The global WAVEWATCH III (WW3) model, operational at the National Centers for Environmental Prediction (NCEP), was first developed for shelf sea applications by Tolman (1991), and is gaining wide acceptance in the wave forecasting community. It is similar to WAM in structure, but incorporates wave-current interactions, a more

sophisticated third-order numerical propagation scheme, new formulations of wind input and dissipation source terms (Tolman and Chalikov, 1996; based on Chalikov and Belevich, 1993). The wind input source function (S_{in}) is calculated at 10-meter height based on the wind speed and direction rather than the friction velocity used in WAM (Tolman and Chalikov, 1996). The dissipation source function (S_{ds}) is defined by a linear combination of two constituents, low-frequency dissipation and high-frequency dissipation. The dissipation of low-frequency swell is assumed to be similar to the energy dissipation due to turbulent viscosity in the oceanic boundary layer, which disappears when the wind and/or high-frequency waves vanish (Tolman and Chalikov, 1996). The parameterization for the high-frequency dissipation is purely diagnostic because wave energy dissipation for this part of the spectrum is poorly understood. An important consequence of these differences is the more rapid wave growth under strong wind forcing in the WW3 model. The WW3 wind input source term becomes negative for waves that travel faster than the wind or at large angles to the wind, is 2-3 times smaller than WAM for fully developed seas, but larger at high frequencies. The FNMOC WW3 model is forced by NOGAPS 3.4 winds at 10-meter elevation and the NCEP WW3 winds are obtained from NCEP's operational Global Data Assimilation Scheme (GDAS) and the Aviation cycle of the Medium Range Forecast model (AVN), assuming neutral stability and adjusted to 10 meter elevation.

The WW3 model solves the spectral action density balance equation in the wave number-directional domain. Like WAM, the WW3 model assumes that the wave spectrum and medium variations (water depth and surface current field) vary on time and space scales much larger than those for a single wave, and thus can only be applied on spatial scales larger than a few kilometers and outside the surf zone because the physics are not valid for regions of severely depth-limited waves. In August 2001, WW3 replaced WAM at FNMOC as the operational wave prediction model.

Global wave prediction models can be validated with data from buoys as well as satellite altimetry. The National Data Buoy Center (NDBC) operates a large number of buoys along the coastlines of the United States and Canada that provide standard atmospheric data (e.g. wind speed and direction) and detailed wave measurements.

These buoys include directional buoys that measure frequency-directional wave spectra and non-directional buoys that measure only frequency spectra. The Coastal Data Information Program (CDIP) of the Scripps Institution of Oceanography also operates directional wave buoys, located mainly along the California coast. Unfortunately, these extensive buoy networks are concentrated along a few coastlines and very little buoy data is available in the central ocean basins and along other continents. Satellite altimetry from ERS-2 and the Navy's Geosat Follow-On (GFO) provide global coverage of more limited wind speed and wave height information. Whereas the NDBC buoys report every hour and CDIP buoys report every half hour, providing near-continuous real time data, polar-orbiting satellites only provide altimetry data every 12 hours.

Previous studies were conducted at NCEP using ERS-2 altimetry data and buoy data to validate both forecasts and hindcasts of the WW3 and WAM models (Tolman, 1998). To use all the satellite data available and have good global coverage, the forecast validation considers a 12-hour window around the valid time, co-locating the satellite and model data with tri-linear interpolation from hourly wave fields. Biases, root mean square errors, and scatter indices were examined for both data sets. Results from the validation with buoy data indicated a large positive bias and high scatter index in the Pacific Regions, especially near Hawaii where sheltering from the islands during the Northern Hemisphere winter interferes with swell propagation from the north. The models had a negative bias in the Atlantic because winds are underestimated close to shore where the AVN model averages winds over land and sea regions. Results from the validation with ERS-2 altimetry data also revealed larger errors during the Northern Hemisphere winter near island chains, such as Hawaii. The NCEP validation study of WW3 and WAM concluded that no significant difference between the two models existed near these island chains. Neither model accounts for the sheltering from the islands because their grid sizes are too large to represent the islands (Tolman, 1998a).

A subsequent WW3 and WAM validation study conducted at FNMOC used 48 NDBC buoys grouped into nine geographic regions and ERS-2 satellite altimetry wave height data. Root mean square error, mean error, and scatter indices were examined on both a global and regional basis. A six-hour window around the validation times was

used, centered on 00, 06, 12, and 18z synoptic times. Results from the validation with ERS-2 altimetry data indicated that WW3 had a smaller wave height error overall than WAM. Results from the validation with the buoy data indicated that, except for Hawaii and the United Kingdom, WAM had smaller errors than WW3. The study also concluded that WW3 lags WAM and the buoy observations for swell arrivals and during increasing wave height events (Wittmann, 2001).

The objective of this thesis is to test the WW3 model implementation at FNMOC and to develop a methodology for comparing spectral information from the models with buoy data. The study was conducted over a six-month period from 1 October 2000 to 31 March 2001, generally considered to be the Northern Hemisphere winter. Preliminary comparisons of the three models are presented at deep water locations. Fifteen buoy locations were used in the study, which include three CDIP buoys located off the coast of southern California and twelve NDBC buoys located in both the Pacific and Atlantic Oceans. The buoys were used as ground truth in evaluating model predictions of swell energy as a function of frequency and time as well as the directional characteristics of the swells.

This thesis is organized into five chapters. Chapter II describes the operational model implementations at FNMOC and NCEP, the various buoy data used in the study, and the model validation methodology. The results for the fifteen buoy locations are presented in Chapter III. Overall model skill is discussed in Chapter IV, followed by a summary in Chapter V.

II. MODELS, DATA, AND ANALYSIS

A. GLOBAL WAVE MODEL IMPLEMENTATION

The three models used in the validation study are WAM (implementation WAM, cycle 4.0, Wittmann and Clancy, 1993) and WAVEWATCH III (WW3) at Fleet Numerical Meteorology and Oceanography Center (FNMOC) and WW3 at the National Centers for Environmental Prediction (NCEP). Until recently, both WAM and WW3 were run in parallel at FNMOC, on a global 1° latitude by 1° longitude grid, with an integration domain extending from 78 N to 78 S. Both models have identical landmass and ice edges. The WAM model is forced by the Navy's atmospheric prediction system NOGAPS 3.4 surface wind stress, and WW3 at FNMOC is forced by NOGAPS 3.4 winds at 10-meter elevation. Both models use a three-hour wind time step. The WW3 model at NCEP uses a 1° latitude by 1.25° longitude grid and a dynamically adjusted ice edge updated daily from NCEP's automated passive microwave sea ice concentration analysis (Grumbine, 1996). The winds from NCEP's operational Global Data Assimilation Scheme (GDAS) and the Aviation cycle of the Medium Range Forecast model (AVN) are adjusted to 10-meter elevation assuming neutral stability. Except for the wind forcing and grid, the NCEP WW3 and FNMOC WW3 models are virtually identical. All three models use approximately the same spectral discretization with 25 frequencies that are logarithmically spaced with an increment factor of 1.1 and 24 directions that span 360° in 15° increments. The wave model time step in WAM is fixed for both the propagation and source terms (20 minutes). The WW3 model uses a variable time step for both propagation and source term integration to increase the model efficiency. The overall time step is one-hour, with a minimum of 5 minutes for the source term and a maximum of 1300 seconds for the propagation time step (Tolman, 1999).

B. BUOY DATA

Fifteen buoys located in deep water in the Atlantic and Pacific oceans were selected for the validation, twelve from the National Data Buoy Center (NDBC) and three from the Coastal Data Information Program (CDIP). The buoys, listed in Table 2.1,

include both directional and non-directional buoys. Figures 2.1-2.3 show the buoy sites and corresponding model grid points used for this study. The grid points for the FNMOC WW3 and WAM models are co-located with each other, but not necessarily with the NCEP WW3 model grid point or the buoy site. The NCEP WW3 model grid points only coincide with three buoy sites.

Name	Number	Latitude	Longitude	Depth	Type
150 nm E. Cape Hatteras	NDBC 41001	34.68 N	72.23 W	4389.1 m	Nomad
Canaveral East	NDBC 41010	28.89 N	78.52 W	841.2 m	Nomad
Georges Bank	NDBC 44011	41.09 N	66.59 W	88.4 m	Nomad
Santa Maria	NDBC 46011	34.88 N	120.87 W	185.9 m	3 m discus
Point Arena	NDBC 46014	39.22 N	123.97 W	264.9 m	3 m discus
Eel River	NDBC 46022	40.72 N	124.52 W	274.3 m	3 m discus
C. San Martin	NDBC 46028	35.74 N	121.89 W	1111.9 m	3 m discus
Monterey	NDBC 46042	36.75 N	122.42 W	1920.0 m	3 m discus
Tanner Banks	NDBC 46047	32.43 N	119.53 W	1393.5 m	3 m discus
California	NDBC 46059	37.98 N	130.00 W	4599.4 m	Nomad
Point Conception	NDBC 46063	34.25 N	120.66 W	598.0 m	Nomad
Christmas Island DWA	NDBC 51028	0.00 N	153.88 W	4755.0 m	3 m discus
Point Reyes	CDIP 02901	37.95 N	123.47 W	320 m	Datawell
San Nicholas Island	CDIP 06701	33.22 N	119.84 W	183 m	Datawell
Point Conception	CDIP 07101	34.56 N	120.78 W	549 m	Datawell

Table 2.1. NDBC and CDIP buoys used in the validation study. CDIP buoys 02901, 06701, and 07101, and NDBC 46042 and 51028 are directional buoys.

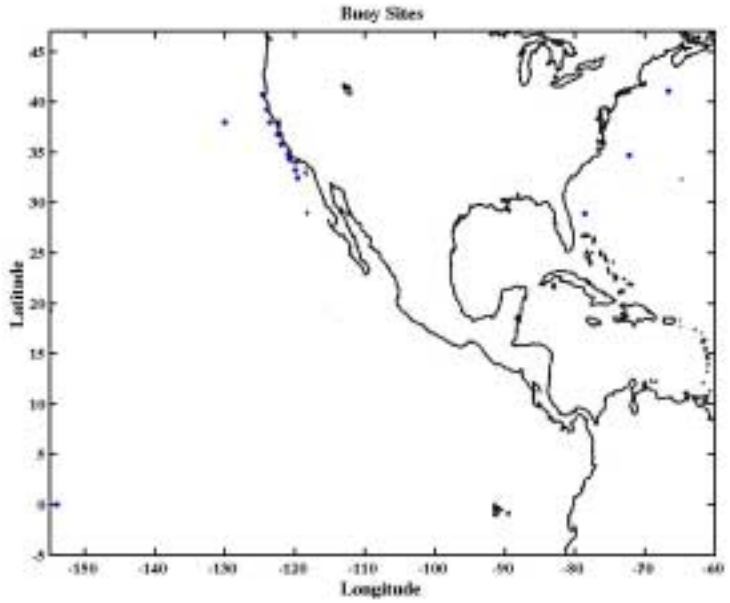

Figure 2.1. Buoy sites (blue dots) used in this validation study.

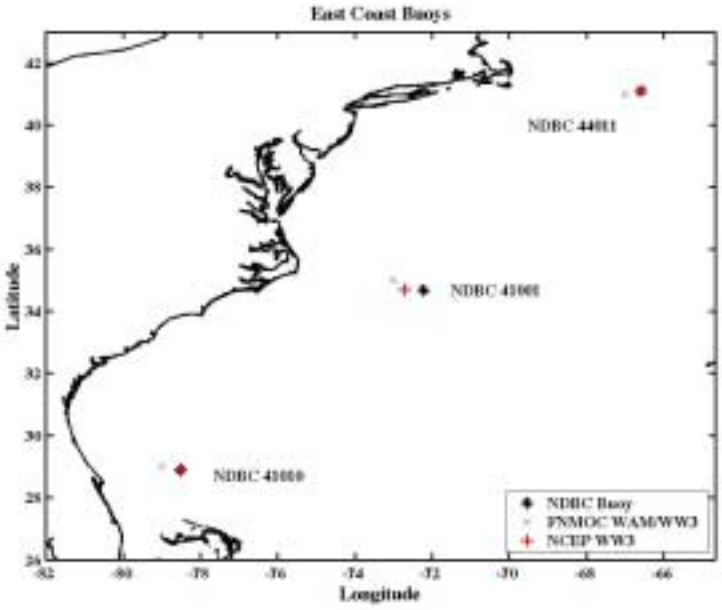

Figure 2.2. East Coast buoy sites and nearby model grid points used in the comparisons.

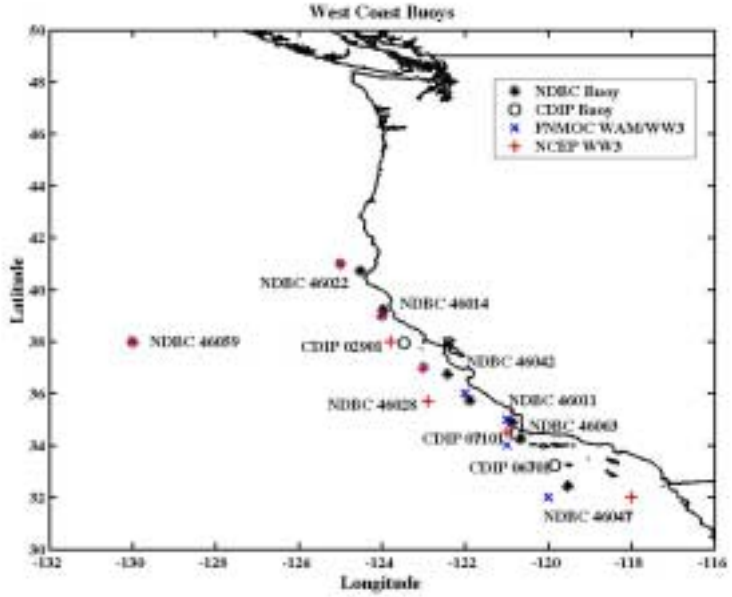

Figure 2.3. West Coast buoy sites and nearby model grid points used in the comparisons.

1. National Data Buoy Center

The National Data Buoy Center operates more than 200 buoys along the coastline of the United States in both deep and shallow waters and provides reports from over 80 other buoys operated by Canada, Meteo France, and the UK Met Office. Three types of

NDBC buoys were used in this study: 6-meter nomad, 3-meter non-directional discus, and 3-meter directional discus (Figure 2.4). All buoys have a heave acceleration sensor that provides a record of the vertical displacement of the buoy during a twenty-minute sampling interval. The buoy processor applies a Fast Fourier Transform (FFT) to the data to transform the temporal data into the frequency domain. The directional buoys have a heave-pitch-roll sensor that measures the sea surface height and tilt in the x-y directions. All buoys report spectral wave density in m^2/Hz for each frequency band (0.03 to 0.40 Hz) every hour, together with various bulk wave statistics such as significant wave height, average wave period, dominant wave period, as well as wind speed and direction measurements, and other standard meteorological data. In addition, the directional buoys also provide a mean wave direction and the directional spread at each frequency.

Figure 2.4. Different types of NDBC buoys. The buoy on the left is a 6-meter nomad non-directional buoy and the one on the right is a 3-meter discus buoy, which can be directional or non-directional.

2. Coastal Data Information Program

The Coastal Data Information Program operates (among other instruments) Datawell Directional Waverider buoys, a small (0.9 m diameter) buoy (Figure 2.5) with excellent wave-following characteristics, equipped with a three-component (x,y,z) acceleration sensor and a two-component (x,y) tilt sensor. The buoy reports frequency spectra and directional moments in the frequency range 0.025 to 0.58 Hz every half hour based on 26-minute long records of x, y, and z displacements. The frequency bandwidths of the spectra are 0.005 Hz below 0.1 Hz and 0.01 Hz above 0.1 Hz.

Figure 2.5. CDIP Datawell Directional Waverider buoy.

C. ANALYSIS METHODOLOGY

Two methods of analysis were used in this validation study. The first method separated and evaluated the energy transported in individual swell events. This method worked well at the Pacific Ocean locations where the wave field was dominated by remote swell arrivals, but was less successful at the Atlantic Ocean sites usually dominated by local wind seas. A simpler method applied at all buoy locations evaluated total wave energy transported in fixed frequency ranges over a fixed time period.

1. Swell Event Analysis

A simple methodology is presented for evaluating swell spectra predictions with spectral buoy data. All three models produce a nowcast (or analysis run) every 12 hours at 00Z and 12Z. The NDBC buoys record data every hour and the CDIP buoys record data every 30 minutes. Data from all buoys were averaged down to one record every three hours to provide smoother records for statistical analysis. Swell events were identified by tracking peaks in the wave frequency spectrum E(f,t) in time. The frequencies, directions, arrival times, and bulk energy of swell events predicted by the models, are compared with the buoy measurements to assess the model performance.

a. Identifying Swell Events

The first step was to identify swell events in the energy spectrum as a function of frequency and time. Energy spectra are often multi-modal, indicating the presence of swells arriving from different sources. Only swell events that were reasonably well separated in frequency were considered for comparison, using a simple criterion

$$\frac{|f_1 - f_2|}{|f_1 + f_2|} \geq 0.15 \tag{2}$$

where f_1 and f_2 are adjacent peak frequencies in the frequency spectrum (see Figure 2.6).

b. Tracking Swell Events

The next step was to track swell events in time as well as frequency. Contour plots (see Figure 3.1 in Chapter III) of wave energy as a function of frequency and time illustrate the evolution of swells from the early arrival at low frequencies to the decay at higher frequencies as time increases (see also Munk et al., 1963). The swell systems arrive at rapid intervals, usually causing the simultaneous presence of multiple swell events that show up as distinct peaks in the spectrum. After tracking the spectral peaks as a function of time, the swell events were terminated when peak frequencies changed by more than 20% over a 12 hour period. For buoys with directional data available, a second criterion was applied. The event was terminated when the mean direction at the peak frequency changed by more than 30° in a 12 hour period. Events lasting less than 48 hours were discarded.

To compare swell events predicted by the models with those observed by the buoy, individual events were matched using the following criteria: (*i*) the model swell mean direction was within 30° of the buoy mean direction, (*ii*) model swell event start/end times were within 36 hours of buoy event start/finish time, and (*iii*) model peak frequency was within 20% of buoy peak frequency. In cases where the buoy was non-directional, only the last two criteria were used. The total wave energy transported past the buoy or model grid point (per unit crest length) over the duration of each individual swell event, was estimated as

$$\rho g \iint C_g(f) E(f) df dt \tag{3}$$

where ρ is the density of seawater, g is gravity, $C_g(f) = g / 4\pi f$ is the group speed, the time integration is over the duration of the event, and the frequency limits are $0.85\, f_p$ and $1.15\, f_p$, where f_p is the peak frequency.

2. Fixed Frequency Range Analysis

To evaluate the model performance in different frequency bands, the buoy data and model output were divided into 48-hour time intervals. The bulk energy transport (equation (3)) was computed over each 48-hour time interval over three fixed frequency intervals: 0.04 to 0.08 Hz, 0.08 to 0.12 Hz, and 0.12 to 0.16 Hz, that represent low-frequency swell, an intermediate range, and high-frequency seas. A relatively long time interval was chosen so that model-data comparisons are insensitive to time lags resulting from the spatial separation of buoy locations and model grid points. If any buoy data or model output was missing the entire 48-hour time period was discarded. Energy transport estimates obtained from the buoy data and model predictions (the analysis runs) are compared in Chapter IV. The accuracy of the buoy estimates is examined by comparing results from co-located buoys in the Appendix.

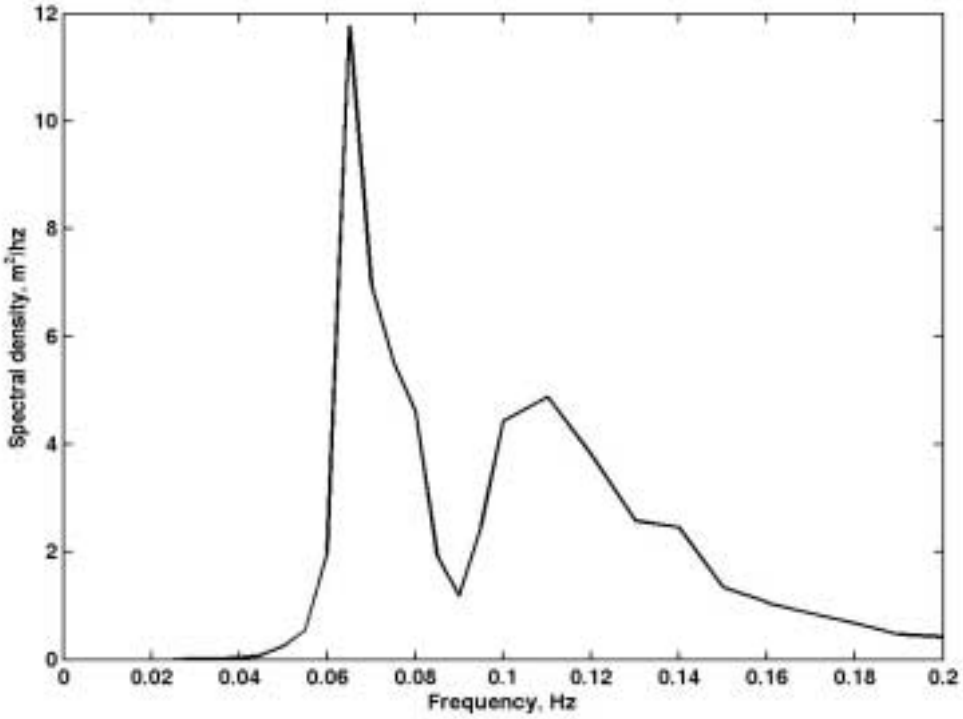

Figure 2.6. Example of a bimodal energy spectrum indicating multiple swell arrivals.

III. RESULTS

A. PACIFIC OCEAN

WAM (FNMOC) and WW3 (NCEP and FNMOC) nowcasts were compared to buoy observations at 12 locations in the Pacific Ocean. Results at 11 buoy locations along the west coast of the United States were generally similar and are illustrated here with comparisons at Point Conception and the California buoy. These results are contrasted with the comparisons near Christmas Island in the Central Pacific region with strong trade winds.

1. Point Conception Results

The swell evolution predicted by the three models is compared with observations from the Point Conception buoy (CDIP 07101) in Figure 3.1. Both WW3 models capture the swell arrivals very well. The WAM model, however, smoothes out the energy and blends two to three swell events into one event. This smoothing may be explained by the fact that WAM uses a first-order upwind propagation scheme that tends to diffuse swell energy as the distance from the generation source increases. The WW3 models using a third-order scheme are expected to be less diffusive. Other differences between WAM and WW3 that may contribute to the superior performance of WW3 in this case are the differences in the wind input and dissipation terms.

The predicted and observed swell peak frequencies and mean arrival directions (at the peak frequency) are compared in Figure 3.2. All three models fail to capture the early arrival of the waves at low frequencies and WAM does not track events into the higher frequencies. Generally, all three models capture frequency and mean direction of swell events very well. WAM mean directions are typically 5-10° further north than the buoy mean directions. During the periods when WAM smoothes multiple events together, the predicted directions do not correspond well with the buoy data. Figure 3.3 shows the energy flux,

$$\rho g \int_{0.85\,fp}^{1.15\,fp} E(f) C_g(f)\, df \tag{4}$$

neglecting directional spreading, versus time for one representative swell event. All models underestimated the energy flux for the event. The models also do not predict the early swell arrival.

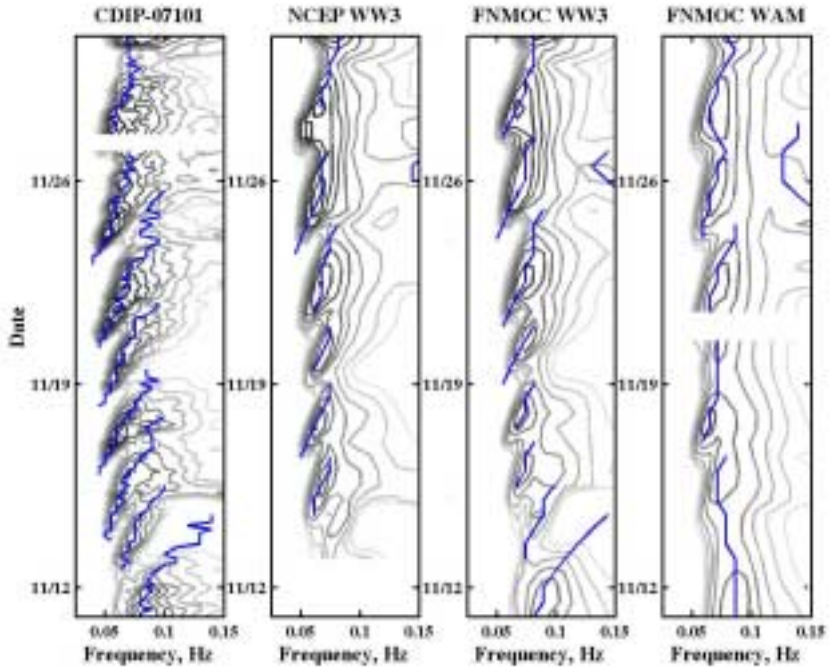

Figure 3.1. Contours of spectral energy versus frequency and time at Point Conception for a 20-day period that is representative of the entire six-month. Gaps in the contour lines indicate time periods for which no buoy observations or model predictions were available. The blue lines indicate events identified and tracked in time.

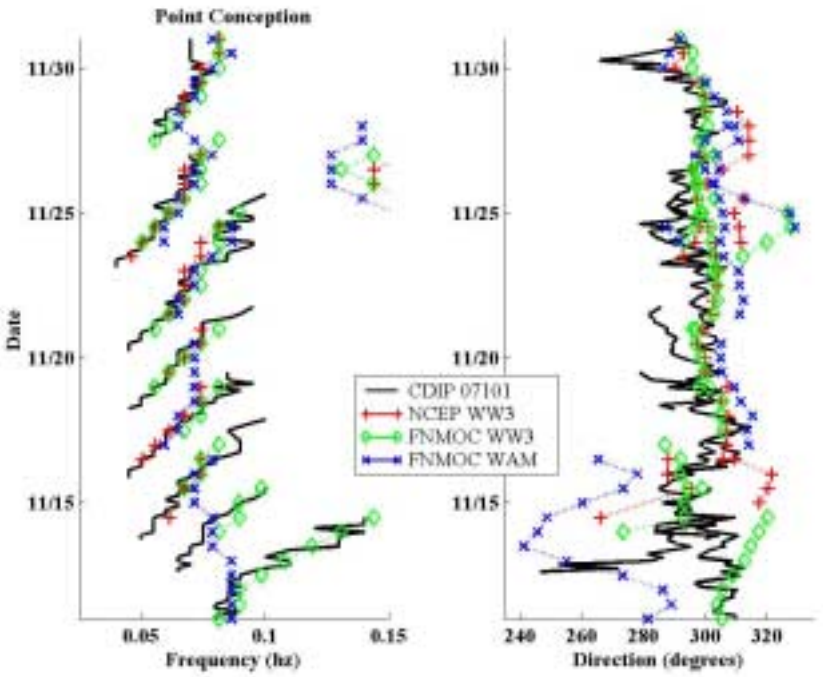

Figure 3.2. Point Conception swell comparisons. Predicted and observed peak frequencies versus time are shown in the left panel. Corresponding mean directions are shown in the right panel.

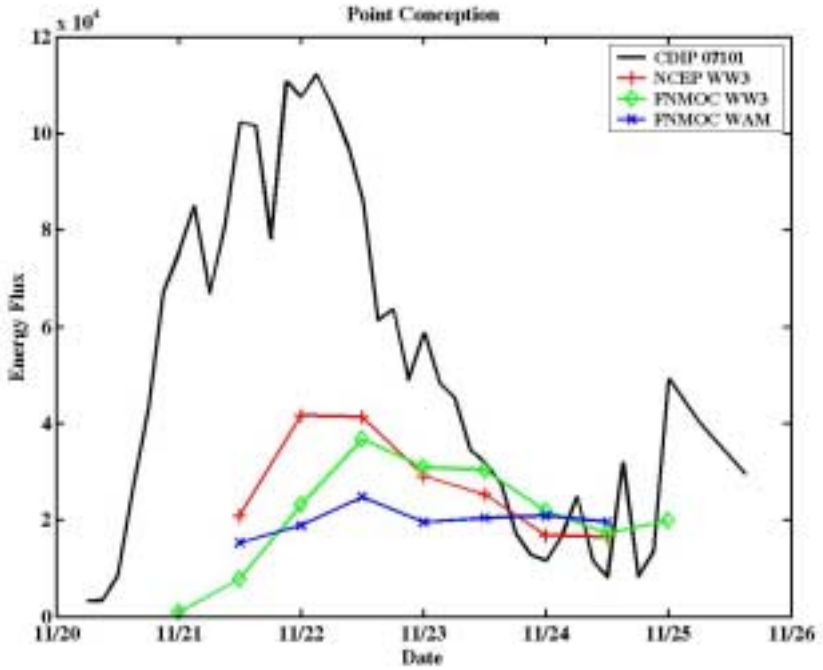

Figure 3.3. Energy flux in W/m for one swell event at the Point Conception site. All three models underestimate the energy flux and do not predict the early arrival of the event measured by the buoy.

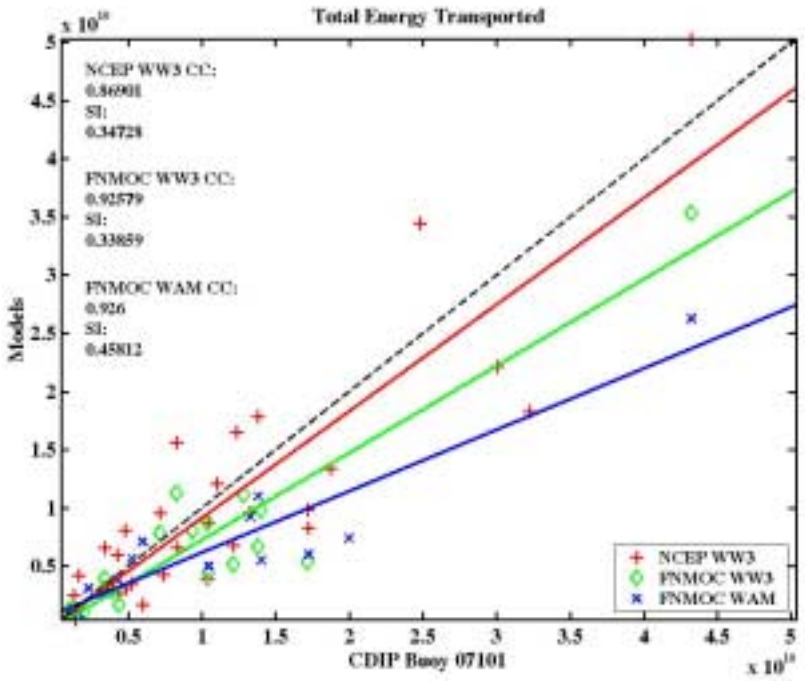

Figure 3.4. Scatter plot of total predicted versus observed energy in J/m transported through the Point Conception site (per unit crest length). Each symbol represents one swell event captured by both the model and the buoy. The solid lines are the best fit lines, the dashed line is the one to one correspondence line. In the legend, CC is the correlation coefficient and SI is the scatter index for the model.

All models tend to under-predict the total energy for Point Conception (Figure 3.4). Both WW3 models have very similar results with lower bias and less scatter than WAM. The scatter index is defined as the root mean square error normalized with the mean observed values. As noted earlier, possible explanations for these differences include the first-order upwind propagation scheme in WAM diffusing energy, a better representation of rapid wave growth under strong wind forcing in the WW3 models, and differences in the dissipation source term.

Results of model-data comparisons in fixed frequency ranges are shown in Figure 3.5. Whereas the NCEP WW3 model predicts accurately the energy at low (0.04-0.08 Hz) frequencies, both the FNMOC WW3 and FNMOC WAM models under-predict the energy by about 50%. There is not much difference between the two FNMOC models which both use NOGAPS for wind forcing, suggesting that the AVN wind forcing used in the NCEP WW3 model better describes the strong forcing conditions that generate low frequency waves.

In the intermediate (0.08-0.12 Hz) frequency range, the two WW3 models are more accurate than the WAM model. The WAM model is biased low in high-energy conditions and biased high in low-energy conditions. As noted above, these errors may be caused by excessive numerical diffusion in the first-order upwind propagation scheme of the WAM model, reducing spatial and temporal variations in wave energy. The difference in the wind forcing between the FNMOC and NCEP models does not appear to play a role in this frequency range.

In the highest (0.12-0.16 Hz) frequency range, smaller differences are noted between the three models. There is little disparity between results obtained with third-order and first-order schemes because waves in this range are primarily generated by local winds and thus less affected by numerical propagation errors.

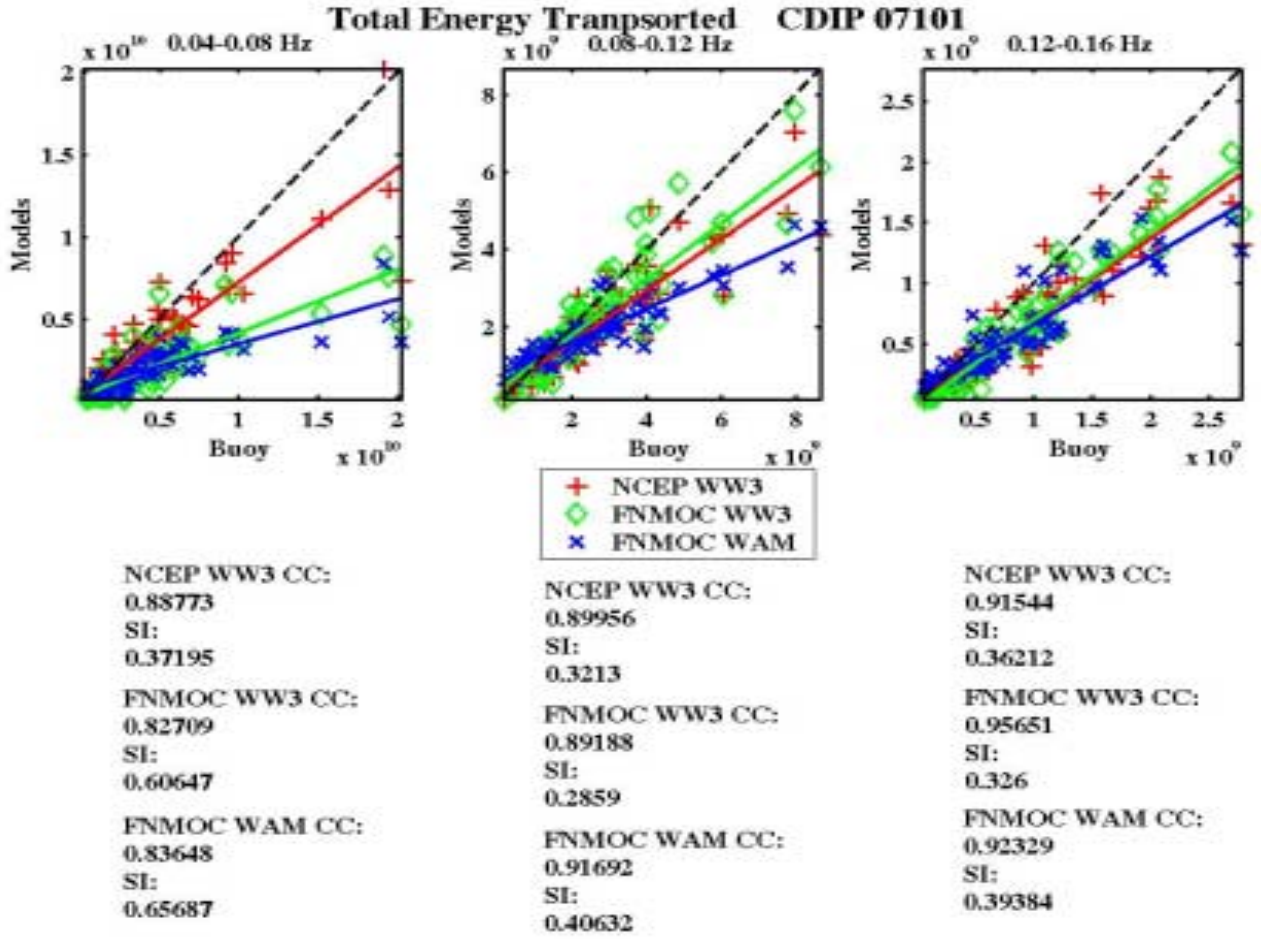

Figure 3.5. Scatter plot of total predicted versus observed energy in J/m transported through the Point Conception site (per unit crest length) for fixed frequency ranges. Each symbol represents a 48-hour period. The solid lines are the best fit lines, the dashed line is the one to one correspondence line. In the text, CC is the correlation coefficient and SI is the scatter index for the model.

2. California Buoy Results

The California buoy is a non-directional NDBC nomad buoy located well offshore, closer to the storm regions in the North Pacific. Figure 3.6 shows the evolution of swell energy versus frequency and time for the same twenty-day period as in Figure 3.1. The spectra are broader than at the Point Conception site because the California buoy is closer to the storm regions. Similar to the Point Conception results, both WW3 models capture the swell arrivals very well, whereas the numerically diffusive WAM model smoothes out the energy and blends two to three swell events into one event. However here, NCEP WW3 resolves the swell events better than FNMOC WW3, particularly the low-frequency waves.

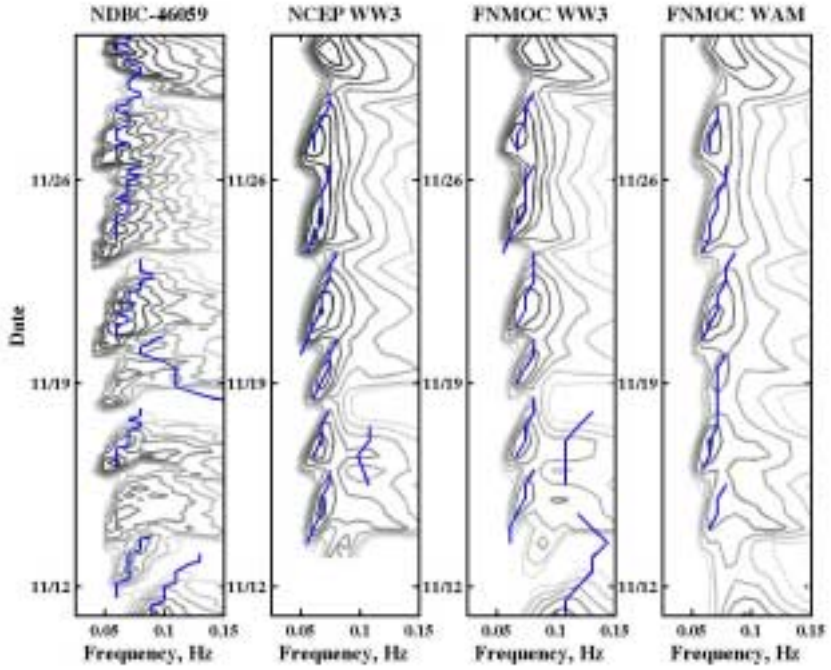

Figure 3.6. Contours of spectral energy versus frequency and time for a 20-day at the California buoy site. (Same format as Figure 3.1.)

The total energy comparisons for all events (Figure 3.7) show considerably more scatter than the results at Point Conception (Figure 3.4). Both FNMOC WW3 and WAM have a smaller scatter index than NCEP WW3. However, only five swell events resolved by the FNMOC WW3 model match events measured by the buoy as compared with 17 for NCEP WW3 and 11 for FNMOC WAM. The scatter indices in this case are not meaningful because they are based on only small subsets of the 47 swell events detected

by the buoy. Often the FNMOC WW3 model predicted swell events similar to those observed in the buoy spectra, but the timing of the swell arrivals was off by more than 36 hours. The NCEP WW3 model over-predicts the swell energy at this site, an error that appears to be associated with the close proximity to the storm generation region.

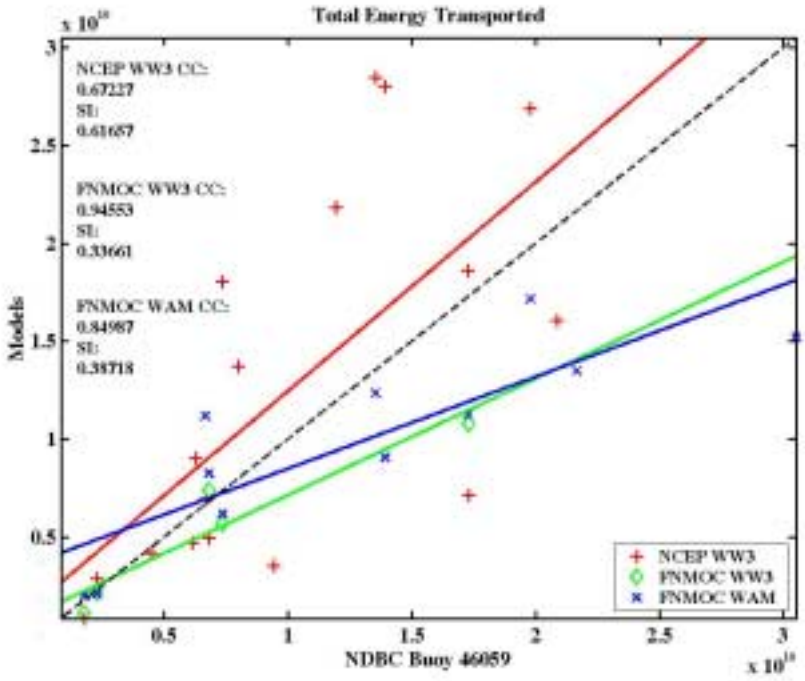

Figure 3.7. Scatter plot of total predicted versus observed energy in J/m transported through the California Buoy site (per unit crest length). (Same format as Figure 3.4.)

Results of model-data comparisons in fixed frequency ranges for the California buoy site are shown in Figure 3.8. These results are similar to the Point Conception site except that the differences between NCEP WW3 and FNMOC WW3 results in the low (0.04-0.08 Hz) frequency range are more pronounced. These very different results obtained with the same wave model suggest that the AVN wind fields used at NCEP better describe the storm systems responsible for low-frequency swells than the NOGAPS wind fields used at FNMOC (eg. the position of the storm center and strength of the winds).

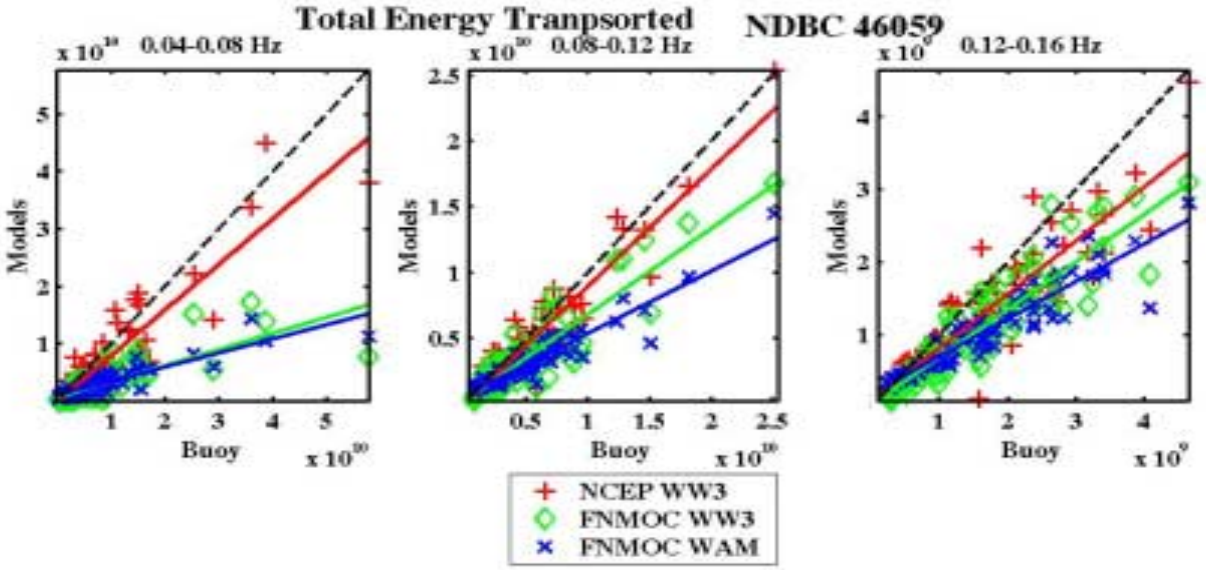

NCEP WW3 CC: 0.91024 SI: 0.34005	NCEP WW3 CC: 0.94007 SI: 0.22865	NCEP WW3 CC: 0.9085 SI: 0.29784
FNMOC WW3 CC: 0.7811 SI: 0.71219	FNMOC WW3 CC: 0.90355 SI: 0.37242	FNMOC WW3 CC: 0.91395 SI: 0.36738
FNMOC WAM CC: 0.87325 SI: 0.71297	FNMOC WAM CC: 0.93964 SI: 0.46356	FNMOC WAM CC: 0.93389 SI: 0.41918

Figure 3.8. Scatter plot of total predicted versus observed energy in J/m transported through the California buoy site (per unit crest length) for fixed frequency ranges. (Same format as Figure 3.5.)

3. Christmas Island Results

Christmas Island is located on the equator south of Hawaii and is under the influence of the trade easterly winds throughout the Northern Hemisphere winter. Figure 3.9 shows contours of swell energy versus frequency and time for a representative twenty-day period. All three models capture the spectral evolution well, with the exception of frequencies greater than 0.1 Hz that were dominated by energetic seas generated by the strong easterly winds that produced a continual fully developed sea with peak frequency of about 0.1 to 0.17 Hz. All models grossly under-predict the energy levels of these seas. At lower frequencies, the observed and predicted wave field was dominated by northwesterly swell. Often the swell energy levels are much lower than those of the equatorial easterly wind seas, and as a result, the analysis is less successful in identifying swell events. For example, notice the swell peak tracked by all three models on 28 January not detected in the buoy data. The contours indicate that the buoy is picking up some energy in the low frequencies, but a more energetic high frequency peak from the equatorial winds masks this low frequency peak.

Figure 3.10 illustrates the high amount of scatter in model predictions in this region. Near Christmas Island, the models do not resolve the coastline, therefore, they cannot model the sheltering effects of the island. In contrast to the California results, FNMOC WW3 appears to do better at Christmas Island than NCEP WW3. Again, the large difference between predictions obtained with the same (WW3) model can only be explained by the difference in the atmospheric forcing. Atmospheric data in the southern hemisphere is generally sparser than in the northern hemisphere, thus larger differences between NOGAPS and AVN wind fields may be expected in this region, which would impact swell generation.

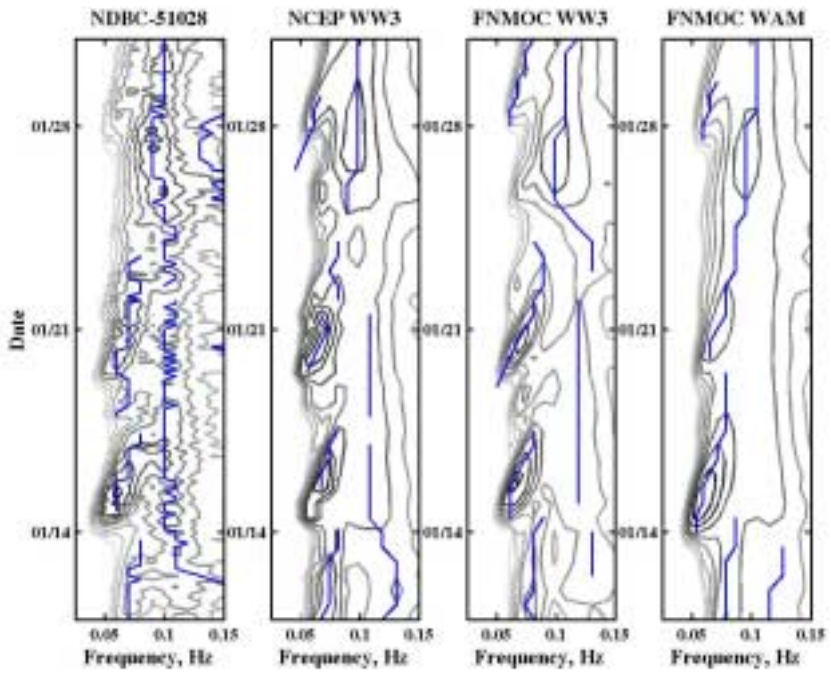

Figure 3.9. Contours of spectral energy versus frequency and time for a 20-day period that is representative of the entire six-month study for the Christmas Island site. (Same format as Figure 3.1.)

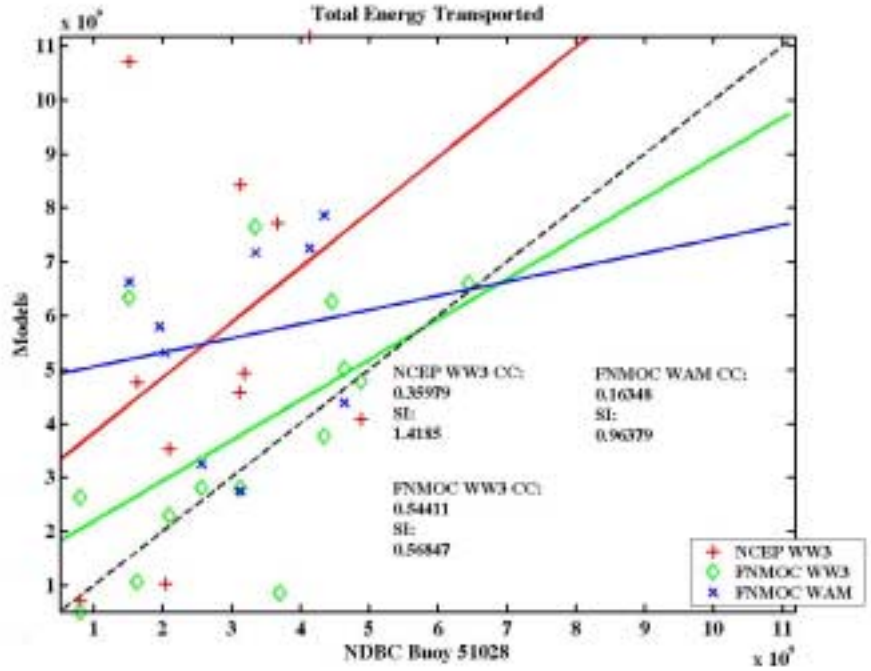

Figure 3.10. Scatter plot of total predicted versus observed energy in J/m transported through the Christmas Island site (per unit crest length). (Same format as Figure 3.4.)

Results of model-data comparisons in fixed frequency ranges for the Christmas Island buoy site are shown in Figure 3.11. Unlike the previous two cases, WAM yields the best results at low (0.04-0.08 Hz) frequencies in this case. The NCEP WW3 model tends to over-predict the energy and the FNMOC WW3 model tends to under-predict the energy in this frequency range. In the intermediate (0.08-0.12 Hz) and highest (0.12-0.16 Hz) frequency ranges, NCEP WW3 predicts the energy more accurately than the other two models. The FNMOC WAM model again is biased high (low) in low (high) energy conditions. The FNMOC WW3 results show the largest scatter index with a consistent negative bias.

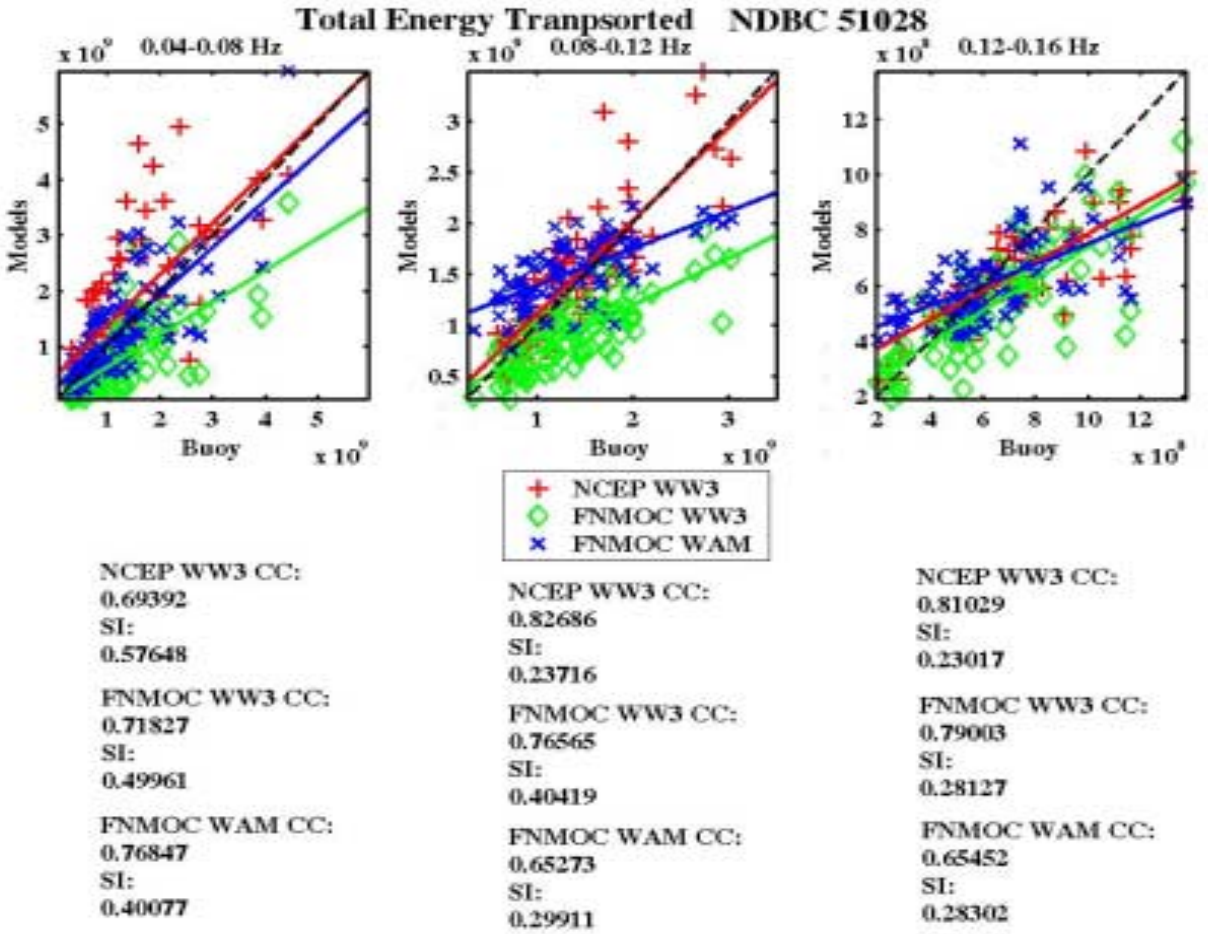

Figure 3.11. Scatter plots of total predicted versus observed energy in J/m transported through the Christmas Island site (per unit crest length) for fixed frequency ranges. (Same format as Figure 3.5.)

B. ATLANTIC OCEAN

All three buoys on the eastern coast of the United States are non-directional NDBC nomad buoys. The swell events were shorter in this region than those seen in the Pacific. Nor'easter storms develop from blocked lows that can originate anywhere from the Rocky Mountains to the Bahamas. The lows move north or northeast and pass across the eastern seaboard into the open ocean. While these storms force a broad spectrum of waves, low frequency (f_p < 0.07 Hz) swell is rarely observed at the Atlantic sites. The spectral evolution predicted by the three models is compared with the observations from the Georges Bank buoy in Figure 3.12. All three models capture the spectral evolution of the seas well. Both WW3 models occasionally predict low frequency swell peaks that are not detected in the buoy data (e.g. 21 and 26 November), possibly because energy levels were relatively low.

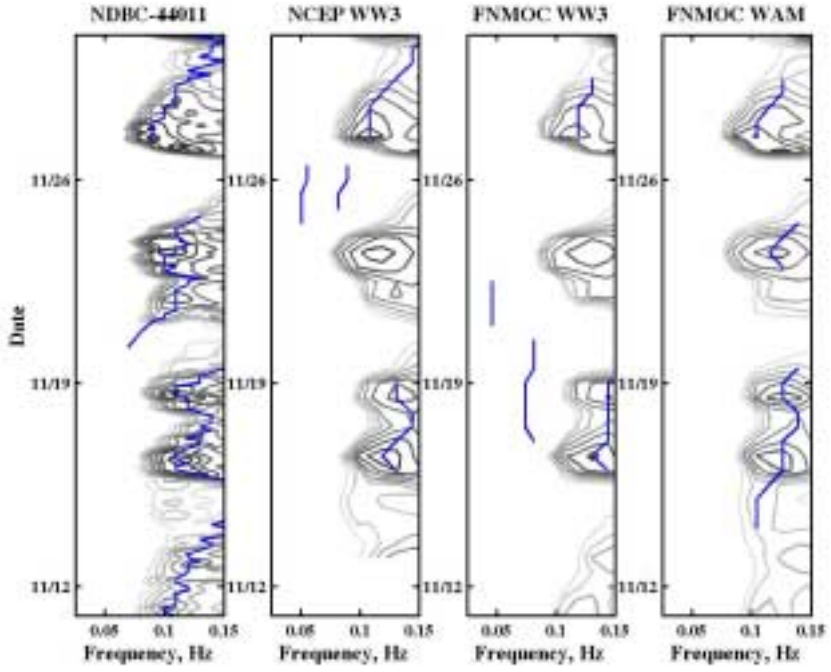

Figure 3.12. Contours of spectral energy versus frequency and time for a 20-day period that is representative of the entire six-month study for the Georges Bank site. (Same format as Figure 3.1.)

Only the fixed frequency band analysis of energy levels was conducted on the three east coast buoys. The results for the Georges Bank are shown in Figure 3.13. In the low frequency range, all three models grossly under-predict the energy, in particular,

WW3 at both forecasting centers. The large errors may be caused in part by the fact that often there is no swell and these comparisons are in the low-frequency tail of the wind-sea spectrum. In the intermediate frequency range, all three models show better results with the lowest scatter index for WAM predictions. The majority of the wave energy is usually contained in the highest frequency range where all three models yield accurate predictions. Here, both FNMOC WW3 and NCEP WW3 have a lower scatter index than WAM.

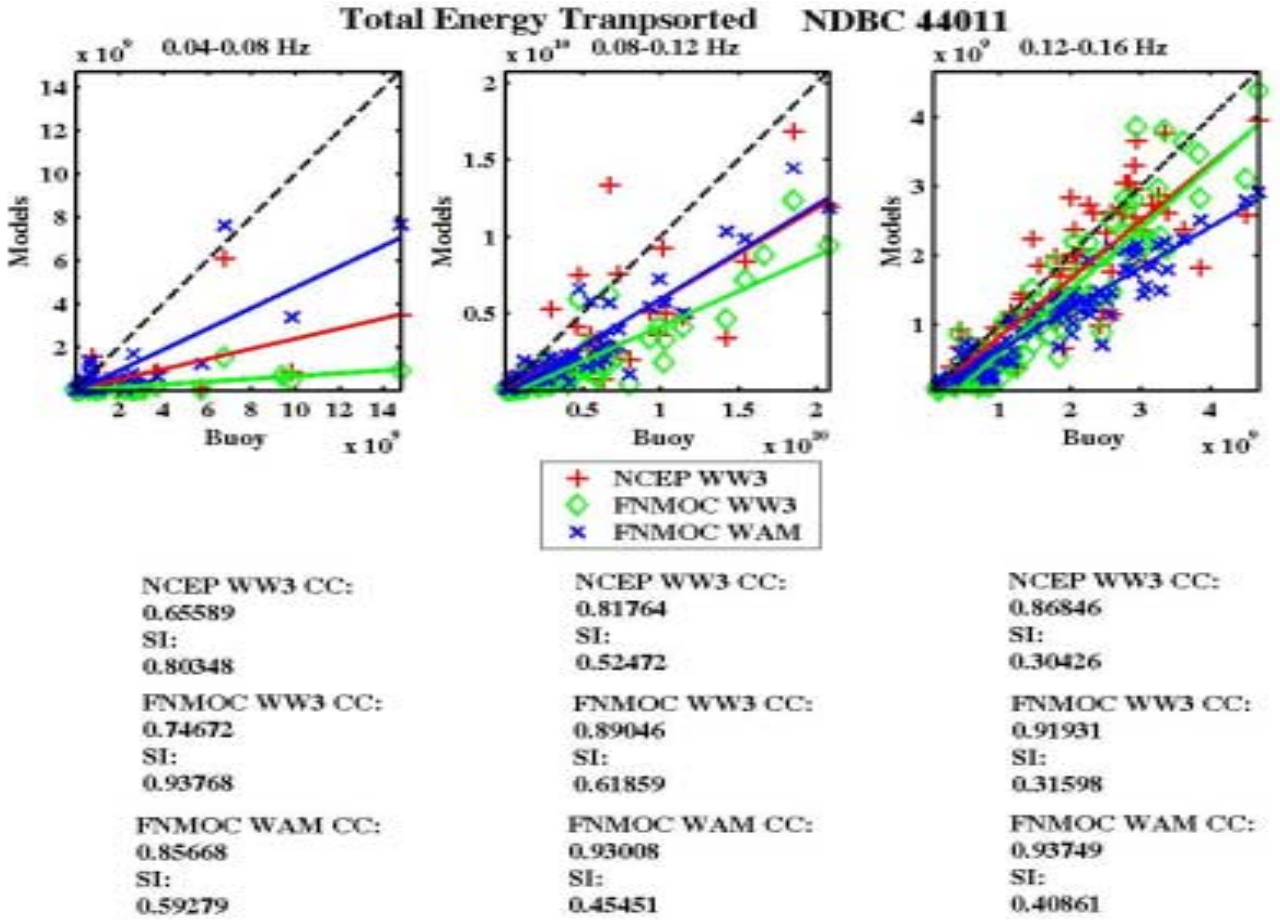

Figure 3.13. Scatter plot of total predicted versus observed energy in J/m transported through the Georges Bank site (per unit crest length) for fixed frequency ranges. (Same format as Figure 3.5.)

IV. MODEL SKILL

A. SWELL EVENTS

The first method of analysis used in this validation study identified individual swell events in the evolution of wave energy in frequency and time. Swell events identified in the model nowcasts were matched to those observed in the buoy data and the total energy transport in the predicted and observed swell event were compared. This method worked well at the West Coast locations, but was less successful at the East Coast and Christmas Island sites, probably due to the predominance of locally generated waves.

Here a summary of the comparisons at all 11 West Coast sites is presented. Scatter indices were computed for the predictions of the total energy transport in each swell event resolved by the model. Figure 4.1 shows the scatter indices for the three models at all buoy sites and Figure 4.2 shows the number of events resolved by each model.

At all sites, NCEP WW3 resolves more swell events than the other two models. The three models have comparable scatter indices that vary considerably from site to site. Results at some buoy sites may be affected by their close proximity to the coast (e.g. 46011, 46022, 46028, and 46063). In some cases, the scatter index is not useful because only a few swell events were resolved (e.g. FNMOC WW3 at 46047 and 46059, and both FNMOC models at 46011). The rather different results obtained with WW3 at NCEP and FNMOC suggests that swell forecasts are sensitive to the wind forcing models. The NOGAPS model at FNMOC is known to have a tendency to under-predict winds associated with deepening storms over ocean basins, consequently, both FNMOC wave models under-predict the wave energy and can miss swell events. The AVN model at NCEP has a high bias for wind speeds less than 7 m/s and low bias for wind speeds greater than 7 m/s. Other possible sources of error could be due to the location of grid points. Not all grid points are co-located with the buoy sites. The grid points used for FNMOC WW3 and WAM are the closest grid points to the buoy sites. The NCEP WW3 model interpolates the spectrum at the West Coast buoy locations from model output at surrounding grid points.

Additionally, some of the differences in model performance at different buoy sites may be related to the type of buoy used in the analysis. For example, two buoys, CDIP 07101 and NDBC 46063, located near Point Conception should yield nearly the same results because the same swells pass through these two buoys. However, the CDIP buoy is directional and the NDBC buoy is non-directional. Adding the directionality criterion to swell event identification (see Chapter II section C.1.b) appears to significantly affect the results. For all three models, the number of swell events that match those of directional buoy 07101 is about twice the number that match those of non-directional buoy 46063.

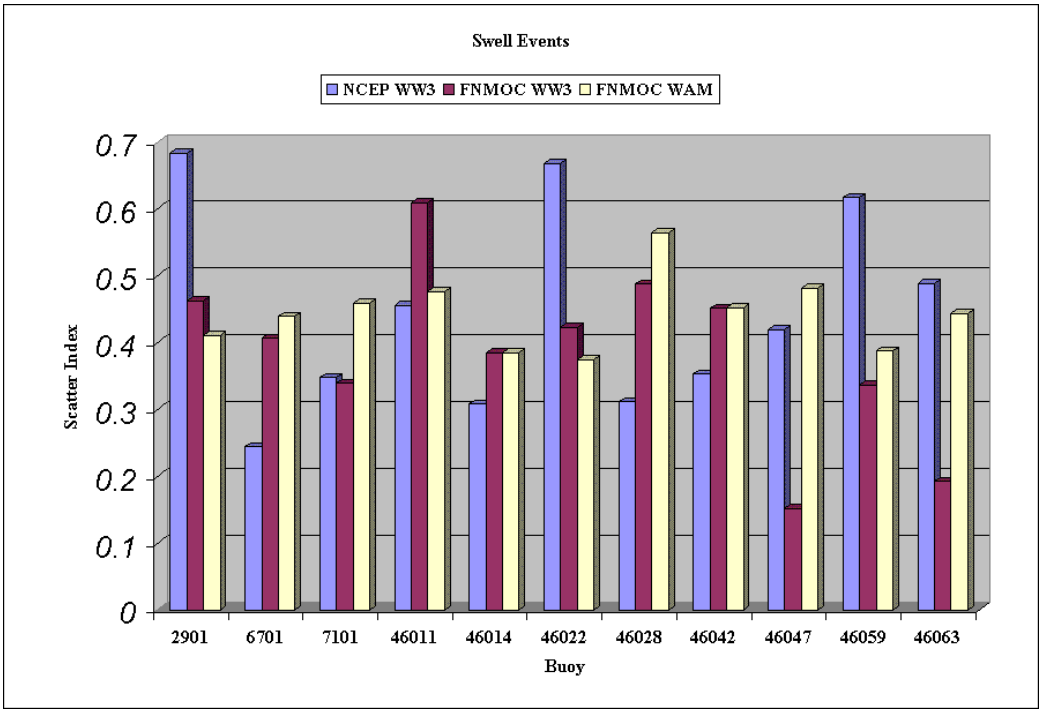

Figure 4.1. Bar graph of scatter indices for all three models at each buoy location. Each bar represents the scatter index of model errors in the energy transport of individual swell events based on comparison with estimates based on the buoy data. The first 3 buoys are the CDIP sites and the last 8 buoys are the NDBC sites.

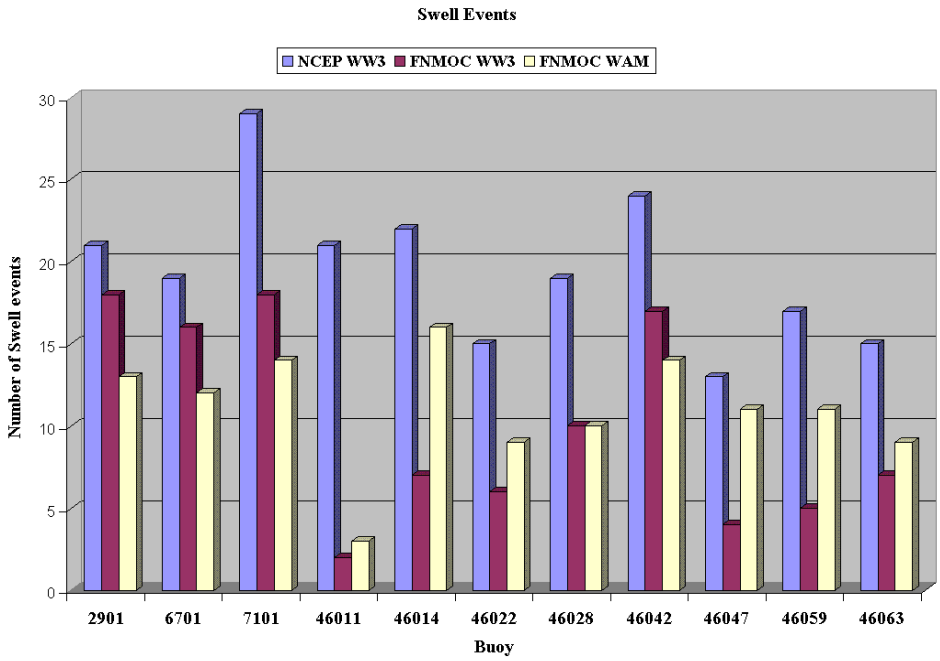

Figure 4.2. Bar graph of the number of swell events resolved for each model at each buoy location.

B. ENERGY TRANSPORT IN FIXED FREQUENCY BANDS

The second method of analysis for this validation study evaluated the total energy transported in three separate frequency bands over 48-hour time intervals. This more robust method, applied at all fifteen buoy sites, compares the models for the entire length of the study, rather than just isolated events. Similar to the swell event comparison, scatter indices for each buoy location are examined in Figures 4.3-4.5 for the three frequency ranges.

In the low-frequency (0.04-0.08 Hz) range (Figure 4.3), errors for all three models are similar at Christmas Island (scatter indices 0.39-0.57), the NCEP WW3 model has a markedly lower scatter index for all the West Coast buoy sites (0.27-0.63) than the FNMOC WW3 (0.43-0.78) and WAM (0.40-0.76) models. On the other hand, the FNMOC WAM model has a lower scatter index for the East Coast buoy sites (0.59-0.76) than the NCEP (0.80-0.90) and FNMOC WW3 (0.93-0.95) models. The large errors in this frequency band at the East Coast sites can be explained by the fact that low-frequency swell is rare in the Atlantic Ocean.

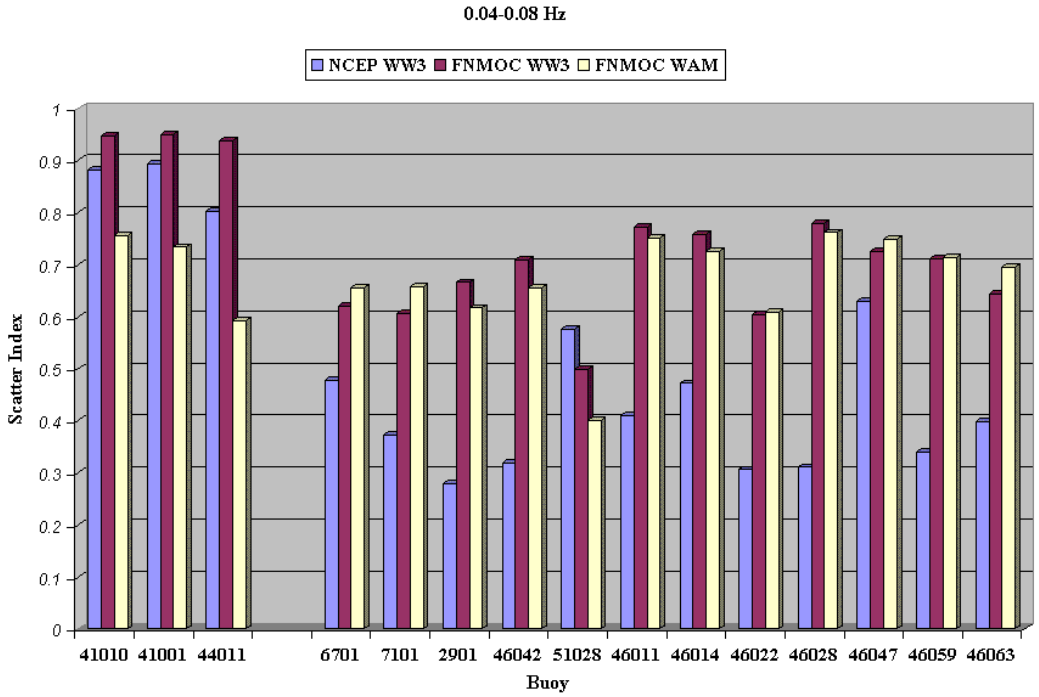

Figure 4.3. Bar graph of scatter indices for all three models at each buoy location. Each bar represents the scatter index of energy transported over 48-hour intervals within the 0.04-0.08 Hz frequency band. The first three buoys are the Atlantic sites, the remaining twelve buoys are the Pacific sites.

In the intermediate (0.08-0.12 Hz) frequency band (Figure 4.4) the differences between the models are smaller. The scatter indices are generally larger at the Atlantic sites (0.45-0.66) than at the Pacific sites (0.22-0.61). The NCEP WW3 model has a lower scatter index than both FNMOC models at two East Coast sites and eight Pacific sites. The FNMOC WW3 model has the highest scatter index at all East Coast sites and seven Pacific sites. As with the 0.04-0.08 Hz frequency band, the two FNMOC models generally under-predict the energy in this frequency band more than the NCEP model, especially in high-energy conditions.

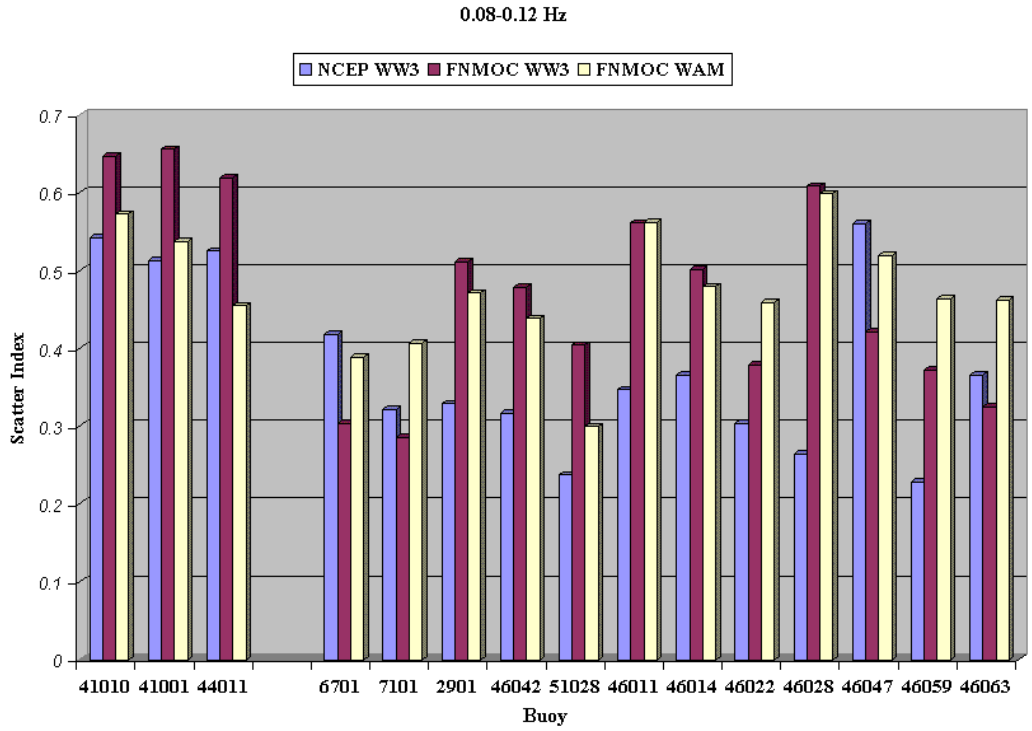

Figure 4.4. Bar graph of scatter indices for the 0.08-0.12 Hz frequency band. (Same format as Figure 4.3.)

In the highest (0.12-0.16 Hz) frequency range, NCEP WW3 generally yields the best predictions with the lowest scatter index at the nine buoy sites (Figure 4.5). However, the differences are small with scatter indices varying between 0.23 and 0.62 for NCEP WW3, between 0.28 and 0.67 for FNMOC WW3, and between 0.28 and 0.61 for FNMOC WAM. At the East Coast buoy sites, the scatter indices for all three models are much lower (0.27-0.47) than in the lower frequency ranges, probably because most of the wave energy at the Atlantic sites is usually in the highest frequency range. At the Pacific sites, the model performance is more variable with the scatter indices that are comparable to those in the intermediate frequency range.

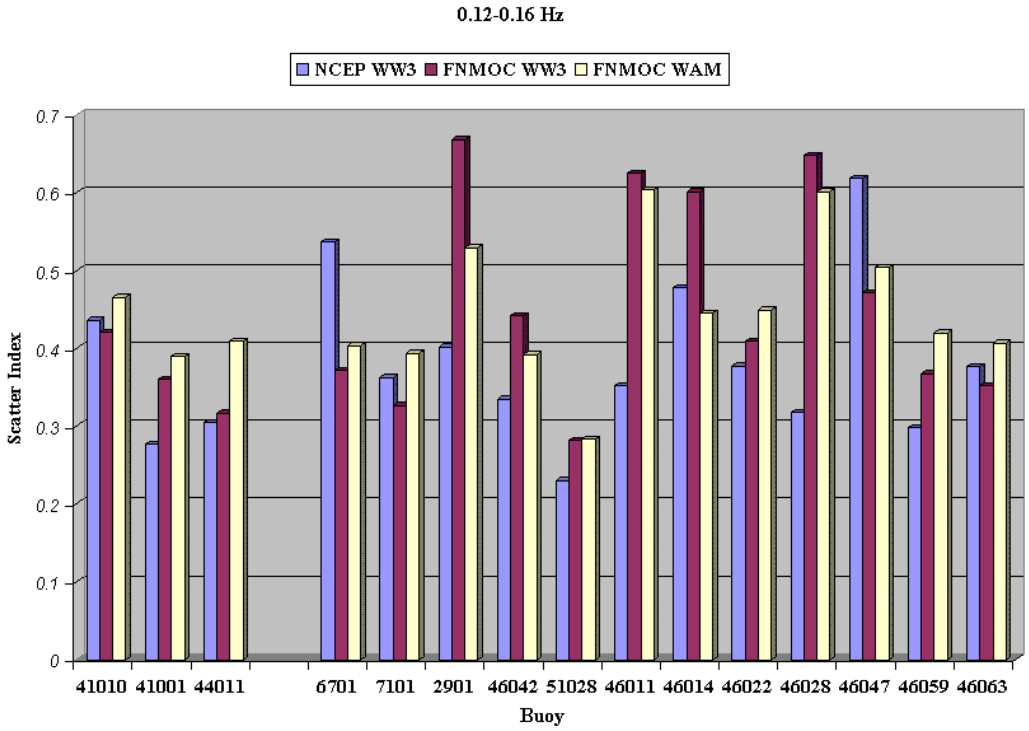

Figure 4.5. Bar graph of scatter indices for the 0.04-0.08 Hz frequency band. (Same format as Figure 4.3.)

V. CONCLUSIONS

The purpose of this study is to develop a methodology for comparing spectral information from global wave prediction models with buoy data and use this method to evaluate and compare operational models at FNMOC and NCEP. The WAM model uses a first-order upwind propagation scheme and well established formulations of the source terms, and is forced by NOGAPS winds. The WW3 model, now operational at NCEP and FNMOC, uses a more sophisticated third-order propagation scheme with new formulations of wind input and dissipation source terms (Tolman and Chalikov, 1996). The WW3 models at NCEP and FNMOC are identical except for the wind forcing. The NCEP WW3 model is forced by GDAS/AVN winds and the FNMOC WW3 model is forced by NOGAPS winds.

Two methods of analysis were conducted over a six-month period for fifteen buoy sites in the Atlantic and Pacific Oceans. The first method of analysis identified and compared individual swell events predicted by the models and observed at the buoys. Swell events were identified by tracking well separated peaks in the frequency spectrum in time. Results indicate that all three models under-predicted the total energy for swell events at both the Pacific and the Atlantic Ocean buoy sites. The WW3 predictions resolved swell events better than the WAM predictions, probably because the third-order scheme in WW3 is less diffusive than the first-order scheme in WAM. The method was less successful at the Atlantic Ocean buoy sites and Christmas Island, where wave spectra were usually dominated by locally generated wind sea (e.g. nor-easters and trade winds).

The second, more robust method of analysis involved separating the spectra into three fixed frequency ranges: 0.04-0.08 Hz, 0.08-0.12 Hz, and 0.12-0.16 Hz. This method worked well at all buoy sites. In most cases, all models under-predict energy in the three frequency bands. Results in the lowest frequency range indicated that NCEP WW3 had the lowest scatter index at all buoy sites. Significant differences between results of WW3 models forced by different wind fields suggest that the GDAS/AVN model provides more accurate wind fields than the NOGAPS model for the dominant Pacific storms that drive low-frequency swell. In the Atlantic, the three models yielded

similar results with large scatter indices owing to the absence of low-frequency swell. In the intermediate frequency range, differences between Atlantic and Pacific results were smaller, as were differences between different models. At most sites, NCEP WW3 yielded the lower scatter index. In the highest frequency band dominated by locally generated seas, all three models yielded similar results with low scatter indices at the Atlantic and most Pacific sites.

APPENDIX

Three different types of buoys, Datawell Directional Waverider, NDBC 3-meter discus, and NDBC 6-meter Nomad, were used in this validation study (Figure A.1). One of each type of buoy was located near Point Conception, allowing for buoy-buoy inter-comparisons. The three buoys have very different hull shapes, as well as different sensors as discussed in Chapter II. The frequency band analysis (Chapter II, section C.2) was conducted on these buoys to compare how they differed in their spectral wave measurements. The results are shown in Figure A.1.

The top three scatter plots compare energy estimates of the 6-meter Nomad buoy 46063 with the Datawell buoy 07101 for the three frequency bands. The Nomad buoy estimates are biased high in the 0.04-0.08 Hz and 0.08-0.12 Hz frequency bands. The scatter index decreases with increasing frequency. The bottom three scatter plots compare the Nomad buoy 46063 with 3-meter discus buoy 46011. There is very little bias and comparable scatter in each frequency band. Overall, the scatter indices in these buoy-buoy inter-comparisons are much smaller than those in the buoy-model inter-comparisons (Chapter V), confirming that the buoys provide reliable ground truth data for the evaluations of the models.

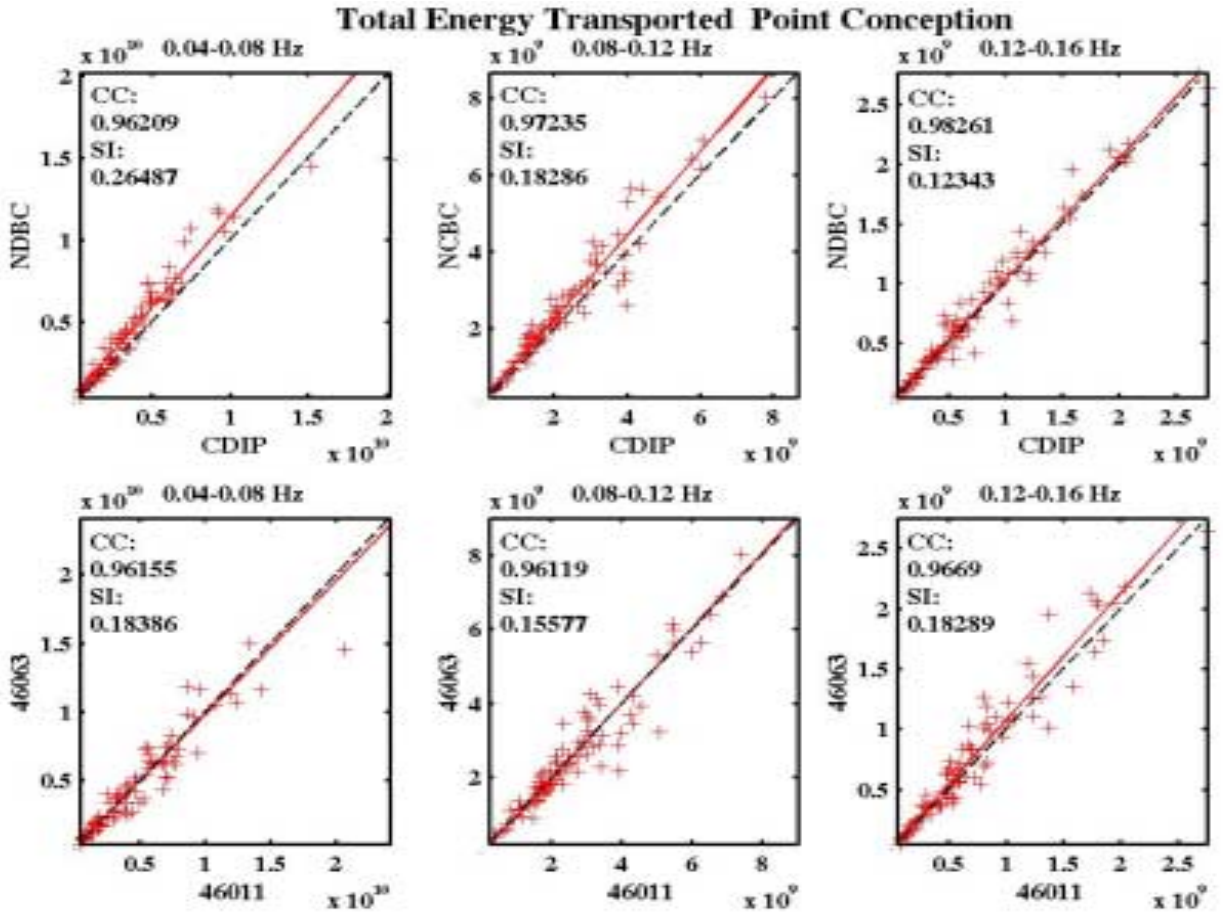

Figure A.1 Six Scatter plots of total predicted versus observed energy in J/m transported through the Point Conception site (per unit crest length) for three frequency bands. The top three scatter plots compare NDBC 46063,a 6 m nomad buoy, with CDIP 07101, a Datawell buoy. The bottom three plots compare the two NDBC buoys, 46063 and 46011, a 3 m discus buoy. Each symbol represents a 48-hour period. The solid lines are the best fit lines, the dashed line is the one to one correspondence line. In the legend, CC is the correlation coefficient and SI is the scatter index for the model.

LIST OF REFERENCES

Grumbine, R.W., 1996. Automated passive microwave sea ice concentration analysis at NCEP. NWS/NCEP/OMB Technical Note **120**, 13 pp.

Komen, G., Cavaleri, L., Donelan, M., Hasselmann, K., Hasselmann, S., and Janssen, P., 1994. Dynamics and Modeling of Ocean Waves. Cambridge University Press, 532 pp.

Munk, W. H., Miller, G. R., Snodgrass, R. E., and Barber, N. F., 1963. Directional Recording of Swell from Distant Storms. Institute of Geophysics and Planetary Physics, **255**, 506-584.

Tolman, H. L., 1991. A third-generation model for wind waves on slowly varying, unstead, and inhomogeneous depths and currents. *J.Phys. Oceanogr.*, **21**, 782-797.

Tolman, H. L., 1992. Effects of numerics on the physics in a third-generation wind-wave model. *J.Phys. Oceanogr.*, **22(10)**, 1095-1110.

Tolman, H. L., and Chalikov, D. 1996. Source terms in a third-generation wind-wave model. *J.Phys. Oceanogr.*, **26**, 2497-2518.

Tolman, H. L., 1998a: Validation of NCEP's ocean winds for the use in wind wave models. *Global Atmosphere and Ocean System,* **6**, 243-268.

Tolman, H. L., 1998b: Validation of a new global wave forecast system at NCEP. In: *Ocean Wave Measurements and Analysis*, B.L. Edge and J.M. Helmsley, Eds., ASCE, 777-786.

Tolman, H. L. 1999a., User manual and system documentation of WAVEWATCH-III version 1.18. NOAA/NWS/NCEP/OMB Technical Note **166**, 110 pp.

The WAMDI Group., 1988. The WAM Model: A third-generation ocean wave prediction model. *J.Phys. Oceanogr.*, **18**, 1775-1810.

Wittmann, P. A. and Clancy, R. M. 1993. Implementation and validation of a global third-generation wave model at Fleet Numerical Oceanography Center., *Proceedings of the Second International Symposium Ocean Wave Measurement and Analysis*, 406-419.

Wittmann, P. A., 2001. Implementation of WAVEWATCH III at Fleet Numerical Meteorology and Oceanography Center., *Oceans 2001 MTS/IEEE Conference Proceedings,*1471-1479.

THIS PAGE INTENTIONALLY LEFT BLANK

INITIAL DISTRIBUTION LIST

1. Defense Technical Information Center
   FT. Belvoir, VA

2. Dudley Knox Library
   Naval Postgraduate School
   Monterey, CA